Structural weaknesses in ice mélange revealed by high resolution ICEYE SAR imagery

William D. HARCOURT,[1,2] Michael G. SHAHIN,[3,4,5] Leigh A. STEARNS,[5] Siddharth SHANKAR,[6]

[1]*School of Geosciences, University of Aberdeen, Aberdeen, UK*

[2]*Interdisciplinary Institute, University of Aberdeen, Aberdeen, UK*

[3]*Department of Geology, University of Kansas, Lawrence, KS, USA*

[4] *Center for Remote Sensing and Integrated Systems, University of Kansas, Lawrence, KS, USA*

[5]*Department of Earth & Environmental Sciences, University of Pennsylvania, Philadelphia, PA, USA*

[6]*PetroStrat, Conwy, UK*

Correspondence: William D. Harcourt <william.harcourt@abdn.ac.uk>

ABSTRACT. The mixture of icebergs and sea ice in tidewater glacier fjords, known as ice mélange, is postulated to impact iceberg calving directly through physical buttressing and indirectly through freshwater fluxes altering fjord circulation. In this contribution, we assess the textural characteristics of ice mélange in summer and winter at the terminus of Helheim Glacier, Greenland, using high resolution (1-3 m) X-band Synthetic Aperture Radar (SAR) imagery from the ICEYE small satellite constellation. The Grey Level Co-occurrence Matrix (GLCM) and statistical variations in pixel intensity down-fjord reveal structural zoning within the mélange matrix in both summer and winter. The boundary between these zones represents the transition between ice concentrations, demonstrating structural weaknesses in the mélange that may persist throughout the year. Furthermore, we compare two iceberg segmentation methods, texture-based vs the Segment Anything Model (SAM). Both techniques detect large (>0.1 km^2) icebergs in summer when pixel variations are larger, but SAM has high iceberg detection accuracy in both seasons. The detected icebergs stabilise near concentration boundaries in the mélange,

suggesting they act as the nucleus of mélange zones and control matrix stability. Our study demonstrates the potential for using high-resolution ICEYE SAR imagery for studying dynamic processes in glaciology and beyond.

INTRODUCTION

Since the early 2000s, the Greenland Ice Sheet (GrIS) has been losing mass at a rate of 233 Gt yr^{-1} (Mouginot and others, 2019; Shepherd and others, 2020; Simonsen and others, 2021; Otosaka and others, 2023). Approximately 66% of this mass loss was attributed to ice discharge (e.g. calving, ice flow) between 1972 and 2018 (Mouginot and others, 2019), which emphasises the need to understand the relative influence of competing processes influencing the stability of tidewater glaciers across the GrIS. A poorly understood process is the role that ice mélange, the granular mixture of icebergs and sea ice at the termini of tidewater glaciers, plays in controlling the position of the ice front over different timescales (Amundson and others, 2020). In winter, ice mélange consists of icebergs bound through sea ice and flows downfjord with resistance by the fjord margins (rigid) (Robel, 2017; Amundson and others, 2020), whilst in summer the mélange matrix is mostly composed of loose icebergs and brash ice (non-rigid) within fjords where ice discharge rates are large (Amundson and others, 2010). The rigidity of the ice mélange matrix impacts the magnitude of the buttressing force it can exert on tidewater glacier termini and has been observed to inhibit fracturing and calving (Amundson and others, 2010; Howat and others, 2010; Burton and others, 2018), whilst sudden mobilisation of a rigid mélange matrix may also act as a precursor to calving events (Xie and others, 2019; Amundson and others, 2020; Cassotto and others, 2021). Further, the influx of freshwater into the fjord through the basal melt of the mélange matrix can increase the heat flux towards tidewater glacier termini (Davison and others, 2020) and enhance submarine melt rates. These processes are likely to vary between fjords and the timescales over which they operate remain largely unknown across the GrIS (Mankoff and others, 2019) yet they could be crucial in modulating discharge rates.

Ice mélange is a highly dynamic, fragmented and mobile phenomenon that varies over a range of timescales (e.g. hours, days, weeks) and hence is difficult to monitor using traditional ground-based and spaceborne sensors. This inhibits our ability to develop an improved understanding of its role in stabilising tidewater glacier calving fronts. Studies investigating ice mélange dynamics are limited to using either coarse-resolution satellite sensors (Foga and others, 2014; Cassotto and others, 2015; Bevan and others,

2019), field sensors with small spatial coverage (Amundson and others, 2010; Peters and others, 2015; Amundson and others, 2020; Cassotto and others, 2021), or physical models with these measurements as input (Amundson and Burton, 2018; Burton and others, 2018; Xie and others, 2019). Both optical and Synthetic Aperture Radar (SAR) imagery have been used to detect the presence and extent of ice mélange in glacial fjords as well as those where it is absent (Foga and others, 2014; Moon and others, 2015; Fried and others, 2018). However, the multi-day revisit period of most satellites and their coarse-resolution imagery (typically >10 m) restricts their ability to assess the more complex dynamics of the mélange matrix such as flow rates, texture changes, and structure. Instead, deep learning methods have been developed to segment components of the fjord system such as ice, snow, and open water (Marochov and others, 2021), with some studies now attempting to detect different elements of the mélange matrix such as individual icebergs (Foga and others, 2014; Shankar and others, 2023), but these methods remain in their infancy. Remote sensing data have proven to be more successful in quantifying the flow of ice mélange downfjord using traditional feature tracking techniques applied to satellite (Amundson and Burton, 2018; Bevan and others, 2019) and ground-based (Peters and others, 2015; Cassotto and others, 2015; Xie and others, 2019) imagery. These measurements have been used to assess mélange rigidity based on the coherence of their flow rates, and when combined with modelling based on granular flow physics, they may be used to quantify the buttressing force on tidewater glacier calving fronts (Burton and others, 2018; Xie and others, 2019). However, current techniques used to monitor ice mélange remain insufficient to fully capture its impact on tidewater glacier discharge

The mélange matrix consists of ice fragments varying in size from centimetres to tens of metres, hence differentiating these features within coarse-resolution satellite imagery and oblique viewing time-lapse sequences is difficult. Further, the flow of ice mélange is granular (Burton and others, 2018) and can disintegrate quickly in response to changing atmospheric and oceanic conditions (Bevan and others, 2019), therefore measurements on the order of hours to days is required to assess its impact on tidewater glacier stability. Measurements of ice mélange at this scale can now be achieved using large constellations of CubeSats and SmallSats that can orbit the entire globe multiple times a day and acquire imagery at centimetre to metre spatial resolution. This supersedes the capabilities of constellations formed of 1-3 satellites (e.g. Sentinel, Landsat), which typically have revisit periods of more than a few days and spatial resolutions of 10 m or more. As of 2023, there are several optical (e.g. Planet) and SAR (e.g. ICEYE, Capella, Umbra) CubeSat and SmallSat constellations in orbit that are used for Earth Observation purposes. However, the

ability of these sensors to map ice mélange extent, features, flow rates and rigidity has not been tested, inhibiting our ability to assess their applicability to ice sheet wide monitoring of the ice-ocean interface and dynamic fjord conditions.

In this study, we evaluate the capabilities of SAR imagery acquired from the ICEYE SmallSat constellation (Muff and others, 2022) to map and monitor seasonal differences in ice mélange conditions at the terminus of Helheim Glacier in Greenland. We focus on the ability of the ICEYE satellite constellation to quantify three pertinent characteristics of ice mélange:

1. Surface characteristics and structure inferred from ICEYE SAR image texture.
2. The distribution of large icebergs in the mélange matrix detected using texture-based and deep learning segmentation approaches.
3. Flow rates of ice mélange determined from feature-tracking techniques to infer rigidity.

STUDY SITE & DATA

We study the perennial ice mélange matrix at the terminus of Helheim Glacier in southeast Greenland (Figure 1). Helheim Glacier, which is the second largest contributor to total GrIS discharge (Mankoff and others, 2019), flows through two branches from the north and south, which coalesce into a ∼6 km wide calving front that is ∼650 m deep and flows at ∼20 m per day in summer. The ice mélange is sustained by a constant influx of icebergs from Helheim Glacier, which have residency times in the matrix of ∼2 months (Moyer and others, 2019). Modelling studies have found a weak dependence of ice mélange on buttressing the Helheim Glacier calving front (Cook and others, 2014). For example, Wehrlé and others (2023) found that weakening of ice mélange can enhance calving activity, but the relationship was highly dependent on external forcing factors and is likely only important on short timescales. In comparison, mélange weakening due to plume melting was found to not impact calving (Everett and others, 2021) but the spatial scale of this process is small and neglects the larger scale fjord pattern. Atmospheric warming is also considered to be a key driver of ice mélange break-up in Helheim fjord (Foga and others, 2014) through wind-driven movement and surface melting. These environmental factors impact the rigidity of the ice mélange matrix, which can promote glacier advance when it is high but can also destabilise a calving front when the matrix is loose and offers no physical support to the terminus (Miles and others, 2016).

We assessed the ice mélange mapping performance of ICEYE SAR imagery at Helheim Fjord in summer

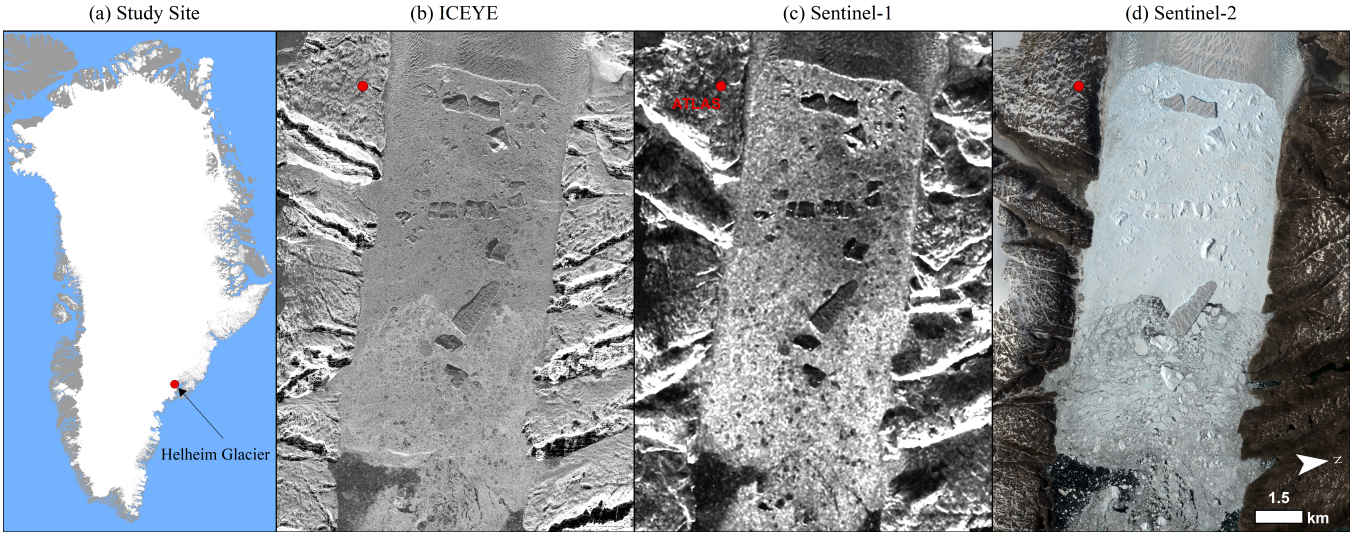

Fig. 1. (a) Location of the Helheim Glacier study site in southeast Greenland. We then show close up images of Helheim Fjord from 20 June 2021 using (b) ICEYE, (c) Sentinel-1, and (d) Sentinel-2. Red dot is the location of the ATLAS instrument.

(2021) and winter (2023) (Table 1). As of July 2025, the ICEYE constellation consisted of 50 satellites (updates here: https://space.oscar.wmo.int/satellites/view/iceye), which enable daily and sub-daily mapping of designated regions on the Earth surface. Each satellite has a SAR payload, which operates at 9.65 GHz (X-band) with a single channel VV polarisation and either a left or right look direction. Here, we acquired SAR imagery in StripMap mode, although several other modes are available (ICEYE, 2023), which has a swath width of 30×50 km and an image area of 1,500 km^2 across a set of incidence angles between 15-30°. The ground resolution of this product is 2.5 m. Images were acquired through tasking i.e. we acquired images at set times when the satellites were passing over Helheim Glacier and its proglacial mélange. In summer (2021), we acquired 3 images in one day and 2 images 7 days later (5 in total) in order to capture the sub-daily conditions of ice mélange when it is most dynamic. In winter (2023), we acquired 10 images between 6 March 2023 and 2 April 2023, covering a period 26 days, to map the rigid structure of wintertime ice mélange. Each image in Ground Range Detected (GRD) format was pre-processed following standard SAR processing workflows in the Sentinel Application Platform (SNAP) software by applying a speckle filter, range-doppler correction, and calibration to γ^0. An example ICEYE image can be seen in Figure 1b and compared to a Sentinel-1 (Figure 1c) and Sentinel-2 (Figure 1d) image of the same region. The high spatial resolution of the ICEYE image enables smaller features such as fractures on the surface of icebergs to be more clearly distinguished.

We compared the ICEYE images to coincident Sentinel-1 scenes in Interferometric Wide (IW) mode,

HH polarisation and 10 m spatial resolution. In 2021, a single Sentinel-1 image on 20 and 28 June were used for a comparison, whilst in 2023 a total of seven Sentinel-1 scenes covering the same time period as the ICEYE image acquisitions were used. To validate data products derived in this study, we used an autonomous terrestrial laser scanner (ATLAS) permanently deployed on the south side of Helheim fjord. ATLAS scans Helheim Glacier and the ice mélange every 6 hours during summer and once per day in winter. The primary data product is a 3D point cloud of the surface.

Table 1. Table of ICEYE SAR images used in this study.

Year	Satellite	Date	Time (UTC)	Orbit
2021	ICEYE X7	20 June	05:28:50	Descending
2021	ICEYE X8	20 June	12:54:06	Descending
2021	ICEYE X2	20 June	13:27:31	Descending
2021	ICEYE X7	28 June	05:28:43	Descending
2021	ICEYE X8	28 June	13:03:39	Descending
2023	ICEYE X12	6 March	03:51:17	Ascending
2023	ICEYE X11	8 March	04:07:35	Ascending
2023	ICEYE X8	12 March	22:54:05	Ascending
2023	ICEYE X12	14 March	03:44:19	Ascending
2023	ICEYE X11	18 March	04:04:34	Ascending
2023	ICEYE X12	21 March	03:47:52	Ascending
2023	ICEYE X11	23 March	04:01:29	Ascending
2023	ICEYE X13	27 March	03:49:20	Ascending
2023	ICEYE X2	30 March	23:29:13	Ascending
2023	ICEYE X7	2 April	15:08:06	Ascending

METHODS

Ice Mélange Segmentation

In this study, we use the following definitions:

Area: A broad classification of a surface type observable in an ICEYE image e.g. land, ocean, glacier, or mélange.

143 *Zones*: Manually defined zones that can be identified in the mélange matrix. Each zone can be
144 differentiated by distinct radar backscatter characteristics.

145 We first delineate the spatial extent of the ice mélange matrix by automatically calculating a threshold
146 based on the distribution of pixel values in the ocean area of the ICEYE image (Figure 2). The ocean was
147 first extracted manually using a shapefile of Sermilik Fjord (Figure 2b). The resulting backscatter image
148 of the ocean is then smoothed using a 2D Gaussian filter, after which the Otsu multi-threshold method
149 (Otsu, 1979) was applied to differentiate between the rough ice mélange matrix and homogeneous ocean
150 and sea ice pixels. In summer, two thresholds are extracted to separate the fjord into 3 areas assuming ice
151 mélange, sea ice, and open water are each present in each image. A similar approach is used in winter, but
152 initially the histogram of the fjord is extracted, lowess smoothed and the number of peaks found. When the
153 distribution is uni-modal, no threshold is applied; when the distribution is bi-modal, two multi-threshold
154 values are found using Otsu's method; when the distribution is multi-modal with more than three peaks, the
155 standard Otsu method of finding 1 threshold is used. In both seasons, the threshold inadvertently removes
156 low backscatter pixels across the mélange such as icebergs with surface melt and the smooth surfaces of
157 flipped icebergs (Figure 2c). This leaves behind holes in the mélange mask, which we fill. Finally, features
158 smaller than 62.5 km^2 (i.e. 2.5 m $\times$ 2.5 m $\times$ 10,000,000 pixels) are removed in order to produce a binary
159 image representing ice mélange and icebergs locked within sea ice (Figure 2d). This ice mélange mask is
160 applied to both ICEYE and Sentinel-1 imagery in subsequent analysis.

161 ## Texture Analysis

162 The spatial variation in pixel values across an image is defined as image texture and varies as the pixel
163 resolution changes. The physical condition of the ice mélange surface alters radar backscatter and therefore
164 image texture, hence analysis of texture changes over time may be used as a proxy for the state of ice
165 mélange. Here, we quantify image texture across the ice mélange matrix in the ICEYE scenes using the
166 following metrics:

167 *Probability Distribution Functions (PDFs)*: Histograms of the ice mélange pixel values are produced
168 for each ICEYE image to characterise the radar backscatter distribution of the ice mélange surface.

169 *Longitudinal Median Profile*: Helheim Fjord is broadly rectangular and for signal processing purposes
170 can be considered an array of pixel values. Here, we use this box array, created by first rotating the

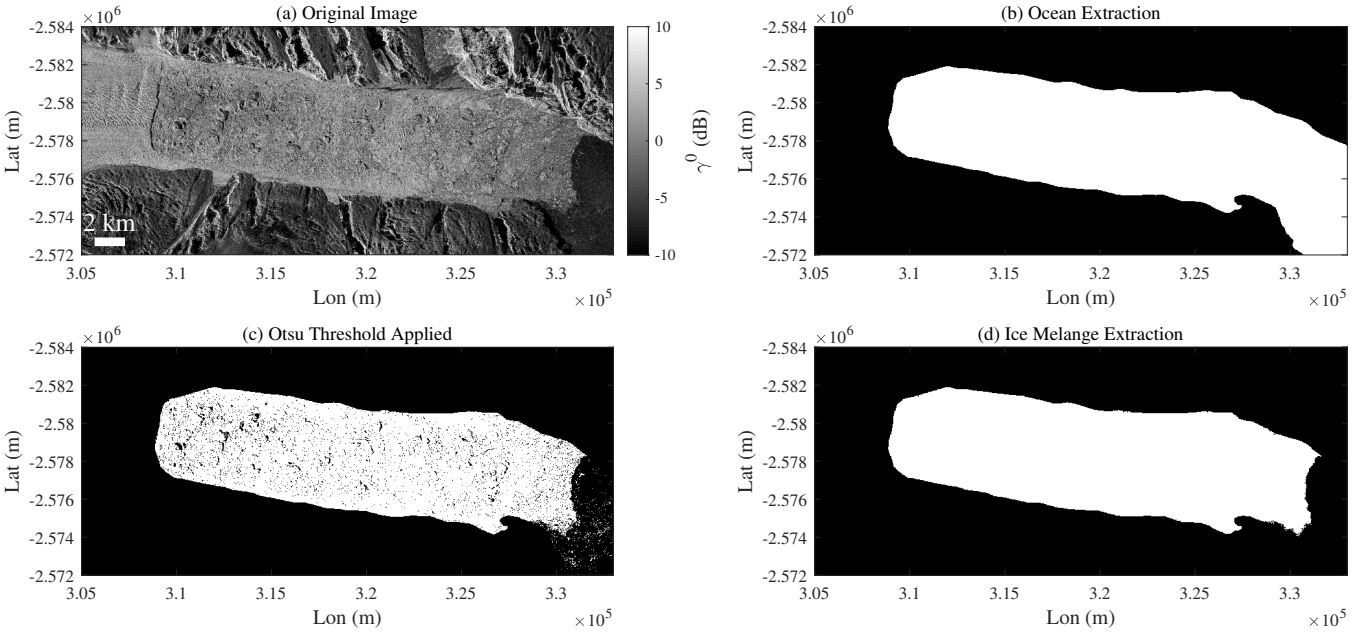

Fig. 2. Extraction of the ice mélange matrix within an ICEYE image. (a) Original ICEYE image from 30 March 2023, (b) manual extraction of the ocean area using a shapefile of Sermilik fjord, (c) application of the Otsu thresholding method, and (d) the final ice mélange matrix extracted from the data processing. In Panels (b), (c), and (d), white represents the presence of ice.

image by 7° due to the angle of the fjord relative to the image acquisition, to calculate the downfjord variation in radar backscatter by extracting the median value of the pixels in each column of the ice mélange SAR image from the terminus of Helheim Glacier to the mélange edge.

Gray Level Co-occurrence Matrix (GLCM): We quantify spatial patterns in pixel values by computing the Gray level Co-occurrence Matrix (GLCM) (Haralick and others, 1973), which calculates the relationship between neighbouring pixels and maps this across the scene. We use GLCM to map the 'Correlation' across each image, which is used to aid iceberg segmentation.

Iceberg Segmentation

Large (>0.1km^2) icebergs within ice mélange are key to bonding sea ice and brash ice together into a granular matrix (Robel, 2017; Burton and others, 2018), whilst they can also act as the catalyst for mélange weakening when they move (Cassotto and others, 2021; Wehrlé and others, 2023). Here, we develop two methods for detecting icebergs within the noisy ice mélange environment and test the methodologies on both ICEYE and Sentinel-1 scenes.

184 *Texture-based Iceberg Segmentation*

The surface features on icebergs within the ice mélange matrix have greater textural variation in the ICEYE imagery compared to Sentinel-1 (Figure 1), which motivated the development of a texture-based segmentation method to detect icebergs in mélange. We first normalised the image by dividing each pixel by the median value in the image column i.e. using the longitudinal mean profile (Figure 3b), which corrects for pixel variation downfjord. The GLCM correlation layer (Haralick and others, 1973) is then computed from this normalised mélange image (Figure 3c). In summer, iceberg edges have low GLCM correlation values as their textural variations reflect the sharp intensity boundary between the iceberg and the mélange. These edges are detected by removing high GLCM correlation values, which generates polygons with holes that are subsequently filled. In winter, this difference is not clear as the entire matrix is frozen. Therefore, to maximise the difference between icebergs and the surrounding matrix, we log-transform each pixel value in the GLCM correlation layer. A threshold is set to remove low pixel values and polygons with holes filled as before. Edges not associated with icebergs are also included in this detection process, hence we filter out these non-iceberg features through a two-stage process. Firstly, the average thickness (T) of each feature is calculated using:

$$T = \frac{A}{L/2} \tag{1}$$

185 where A is the feature area and L is the feature perimeter length. Then, all features smaller than a
186 manually defined threshold are removed. Here, we used 25 pixels ($25 \times 2.5 = 62.5$ m) as the threshold,
187 which balances the need to remove small icebergs whilst still retaining pixels representing large icebergs.
188 Secondly, a bounding box around each feature is computed and the density of points within it calculated.
189 We remove features with a low pixel density (<0.3 pixels per box) as we assume they represent a random
190 collection of pixels rather than an iceberg. The result of this whole process is a binary image of iceberg
191 locations.

192 *SAM Iceberg Segmentation*

193 We use the Segment Anything Model (SAM) developed by Meta to detect icebergs within the ice mélange
194 matrix (Kirillov and others, 2023). SAM is a foundational model trained on millions of images and has pre-
195 viously been shown to demonstrate good performance for detecting glaciological features such as crevasses
196 and icebergs (Shankar and others, 2023). SAM can run either with no prompts, where the model segments

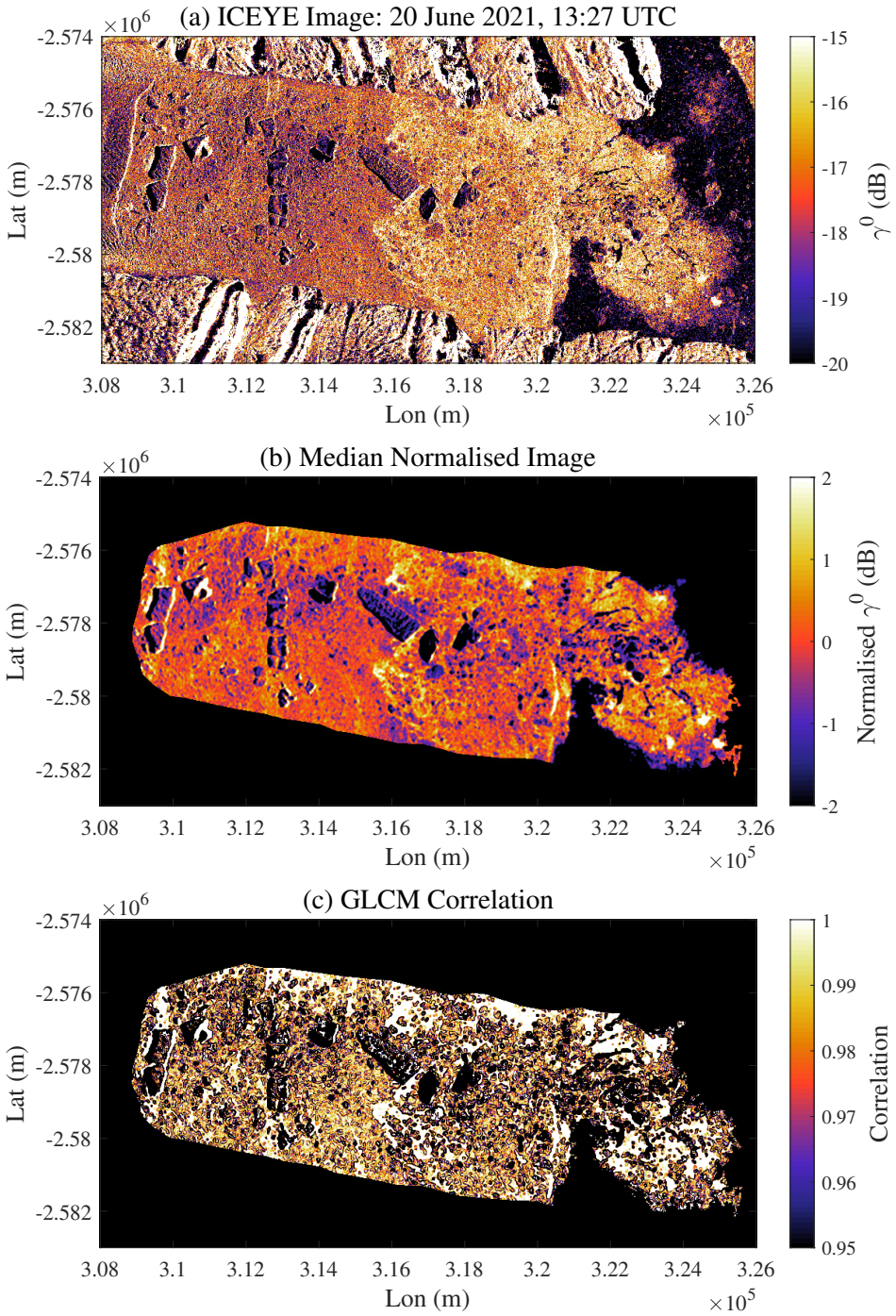

Fig. 3. (a) ICEYE image from 20 June at 13:27 UTC, colored by radar brightness. (b) Gaussian smoothed image with the ice mélange area extracted (see section 'Ice Mélange Segmentation') and normalised by the median longitudinal profile of the mélange matrix. (c) GLCM correlation layer calculated from the normalised mélange area.

features with no a priori information, or with prompts, whereby the user provides context on where there are certain features in the scene. SAM also requires 8 bit 3 band imagery, hence we first convert our ICEYE and Sentinel-1 imagery into .png files before running SAM. We also only use the HH band from the

Sentinel-1 imagery, since ICEYE is single channel. Here, we use no prompt SAM due to the slightly higher F1 score quantified by Shankar and others (2023) for iceberg segmentation in a mélange compared to the prompted score. To increase the number of icebergs segmented, we adjusted the "zoom" of our images by patching each scene into 5 km x 5 km squares. Land mask artifacts can be created when adjusting the "zoom". We ignore these large artifacts, which results in misclassified segmented areas, by manually filtering them out.

Validation

To quantify the accuracy of the segmentation results we compared the output of SAM with labels of icebergs that were delineated manually. The ICEYE images were used to derive the manual labels. We delineate a range of iceberg types within the rigid mélange matrix to achieve a diversity of sizes for validation. We did not delineate icebergs in the non-rigid matrix because there are large quantities of smaller icebergs such as growlers and bergy bits, which are extremely difficult to track individually. Even for those which can be tracked there is likely to be human error leading to missed occurrences that would lead to a lower accuracy that are not representative of the methodology, but rather just human bias. Comparison of the outputs to the manual labels was computed by calculating the F1 score (Shankar and others, 2023):

$$precision = \frac{TP}{TP + FP} \tag{2}$$

$$recall = \frac{TP}{TP + FN} \tag{3}$$

$$F1 = \frac{2 \times precision \times recall}{precision + recall} \tag{4}$$

where TP is a true positive, FP is a false positive, and FN is a false negative. A TP represents an instance when a pixel that is classified as part of an iceberg overlaps with the location of a manual label. The F1 score ranges between 0 and 1 and is the harmonic mean of the precision and recall. The closer to 1 the F1 score is, the better the match of the SAM outputs to the manual labels and therefore the better the model performance. The F1 score for the texture-based method is unreliable due to the impact of smaller icebergs on the detection results and so this method is assessed qualitatively.

Ice Mélange Dynamics

We mapped the velocity of the proglacial mélange using the Image GeoRectification And Feature Tracking Toolbox (ImGRAFT) (Messerli and Grinsted, 2015). It was not possible to compute velocities in summer 2021 as the mélange matrix was non-rigid, hence we focus on the rigid matrix in winter 2023. The DEM used for the range-Doppler correction applied in pre-processing was set to 0 over the mélange to avoid geometric errors of an outdated DEM. Each ICEYE image was then subset covering the glacier terminus, Helheim Fjord and the northern part of Sermilik Fjord. The velocities were calculated from image pairs with time differences of 2-4 days, hence we computed a total of 8 velocity maps. The images were coregistered within SNAP by stacking image pairs together. We used a template window size of 20×20 pixels and a search window size of 150×150. The Normalised Cross Correlation (NCC) method was employed to match image features. The ICEYE velocities over the mélange matrix were validated using the velocities computed from the ATLAS 3D point clouds. Each point in the ATLAS point cloud was tracked automatically and the resulting displacements averaged within individual grid squares of 100×100 m, hence the final displacement map is a grid over the mélange at 100 m resolution.

RESULTS

Ice Mélange Texture

The texture of the ice mélange matrix in ICEYE SAR imagery differs between summer and winter (Figures 4 and 5). In winter, when temperatures are below freezing and the mélange matrix is more rigid, the PDFs are consistently Gaussian among the 10 images with differences only in their shape, standard deviation and mean value. We consider the impact of snow on surface texture to be negligible given that X-band penetration into dry snow can range between 1 and 7 m (Millan and others, 2015; Huang and others, 2021). Of the 10 winter images, the standard deviation differs by only 2.5 dB and averages at 13.4 dB, indicating the texture is stable over the 26 day winter study period. In comparison, the PDFs for summer are much more variable. Whilst one of the mélange PDFs is Gaussian with a mean γ^0 of -17.1 dB, two of the PDFs are negatively skewed and another two have bi-modal distributions. The negatively skewed distributions indicate that there is an increase of smaller γ^0 values in the image related to changes in mélange surface characteristics. The presence of a bi-modal distribution implies that at least two zones can be identified in the mélange matrix, which may be related to changes in ice density and composition. The mean values of

the PDFs in summer are consistently below -5 dB whilst the mean values of the winter PDFs are consistently above 0 dB, providing a useful metric through which to differentiate between summer and winter mélange conditions. The variation in the γ^0 distribution over 7 days illustrates the large variability of ice mélange image texture in summer. In comparison, the consistent Gaussian distribution in winter demonstrates that the mélange matrix maintains a random mixture of ice types over approximately one month.

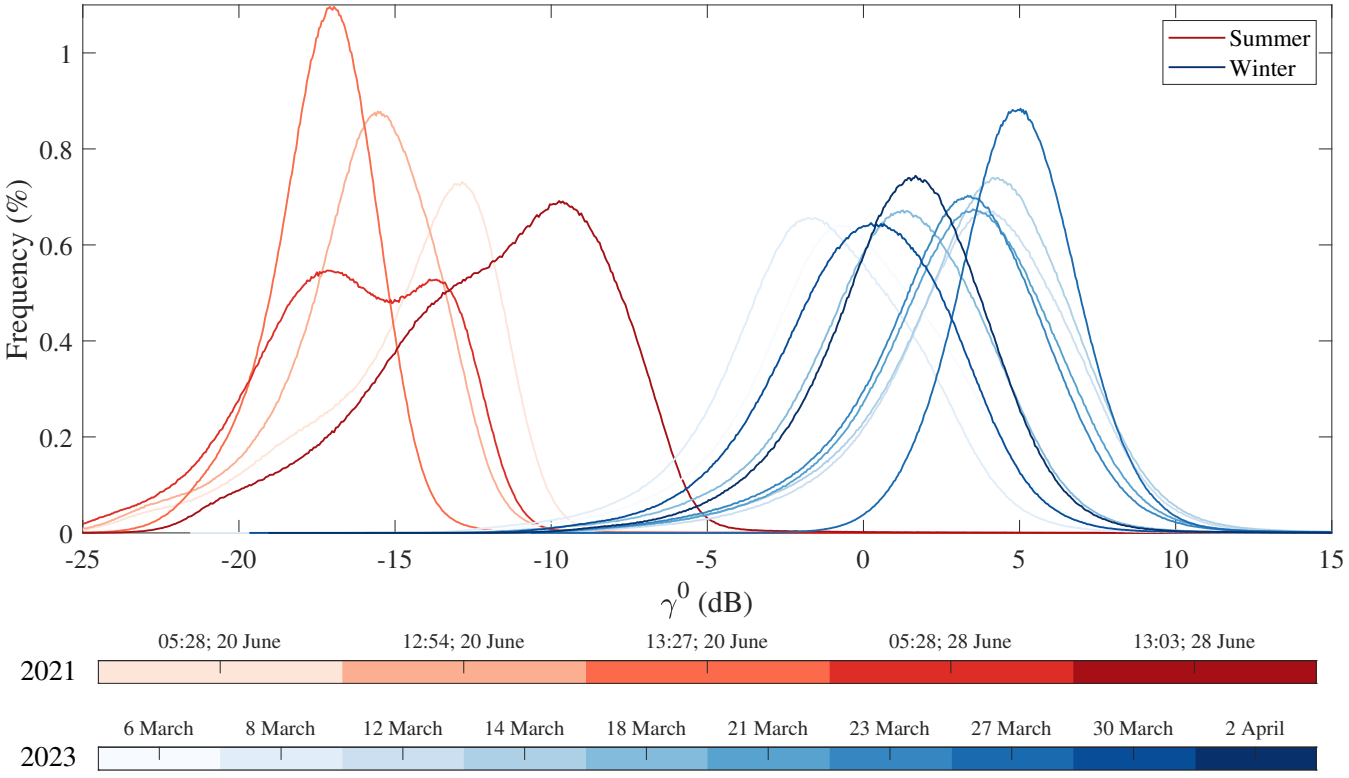

Fig. 4. Summer (red) and winter (blue) Probability Distribution Functions (PDFs) for ICEYE γ^0 values over the Helheim Fjord ice mélange matrix.

There is also spatial variability in ice mélange texture as evidenced by the changes in normalised median pixel values downfjord (Figure 5). These longitudinal profiles reveal zones within the mélange in both summer (Figure 5a) and winter (Figure 5b). In summer, we detect 4 zones. In the first 3 km, pixel values remain consistent before entering zone 2 where there is a rapid rise and plateauing of the the pixel values. Zone 2 is the largest zone and extends between 3 km and 11 km from the terminus. Zone 3 represents the edge of the mélange and varies significantly between each image and then zone 4 represents the ocean that sometimes contains ice to form part of the matrix. In comparison, we detect only two clear zones in winter. The first extends from the terminus to 11 km from the terminus and is characterised by a slow rise in pixel values. In Zone 2, there is a distinct change where pixel values fall at a similar rate. Whilst sub-zones may exist in both summer and winter, these broad zones appear to be consistent in all

images in their respective seasons. There is greater spatial variability in summer compared to winter given that there are 4 zones compared to 2. In contrast, winter texture is more variable at a small scale as evidenced by high frequency variations that are superimposed on the lower frequency pattern of zones that we have identified. While some zone transitions are distinct and discernible from the median profiles alone, the summer transition between sparse melange to open ocean is more gradual and in these situations we refer back to the original 2D image to delineate the zone boundary.

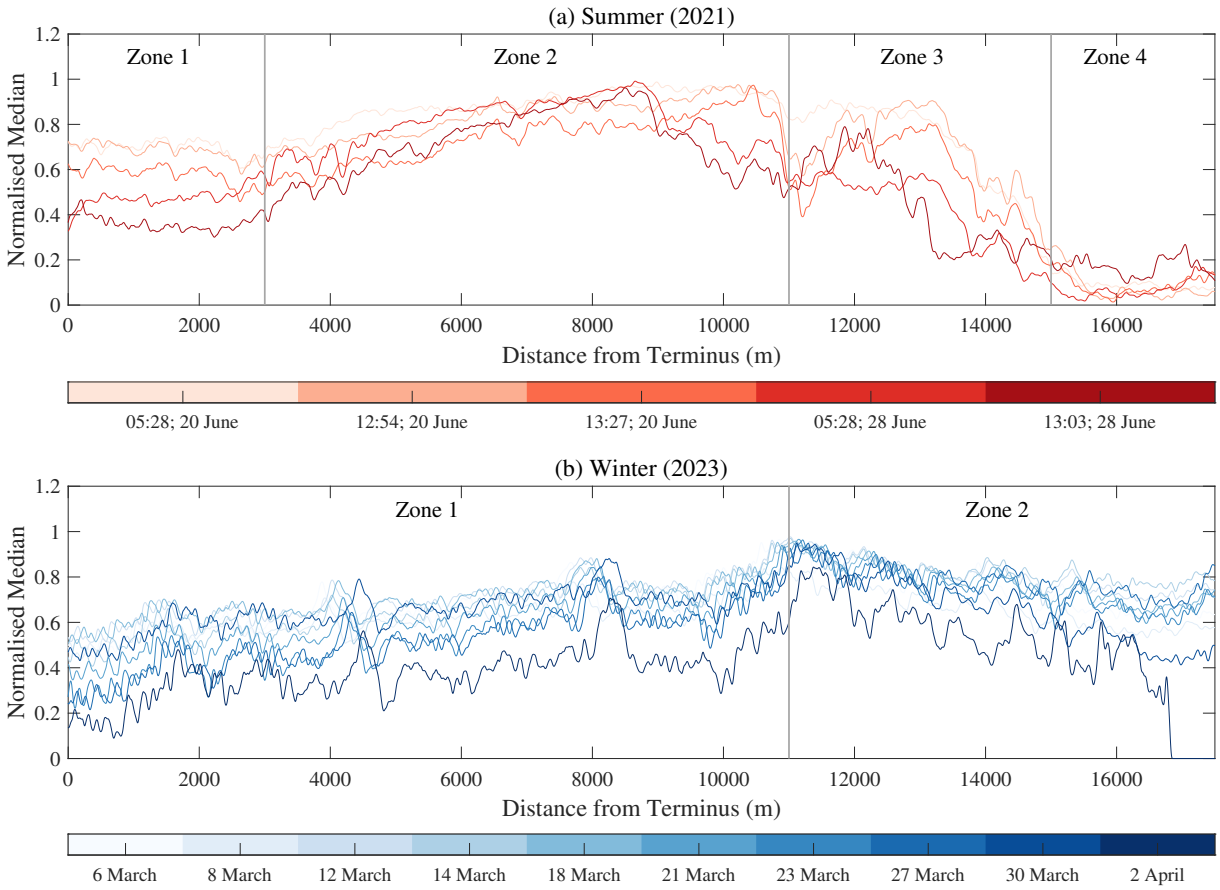

Fig. 5. The median pixel value along each column of the image in a) summer (red) and b) winter (blue). These have been normalised by dividing through by the maximum pixel value along each longitudinal profile. Manually defined zones in the profiles have been indicated.

Iceberg Segmentation Performance

Iceberg detection results for ICEYE images using the texture-based method in summer and winter are shown in Figure 6. In summer (2021; Figures 6a and 6c), the texture-based method is able to detect the large icebergs in the mélange matrix, although noise surrounding the pixels led to misclassification near their boundaries. The two icebergs near the terminus are correctly delineated, whilst the section of three

icebergs further downfjord are detected although there is more noise in the detection results here. The large iceberg beyond 7 km from the terminus is correctly detected. Beyond this section, a collection of smaller icebergs have been detected, although we suspect many have been removed during the filtering process. In comparison, iceberg detection in winter (2023; Figures 6b and 6d) is of lower quality. Whilst the method correctly detects small icebergs across the matrix, it misses several of the large icebergs near the terminus. The texture analysis in the previous section demonstrated how the winter matrix has a Gaussian PDF and therefore pixel values are random. Therefore, differentiating icebergs within the mélange was not possible based on the current texture-based detection method. It was only possible in summer due to the large variations in texture between icebergs and the surrounding mélange. In summer, large icebergs can be more readily detected whilst in winter it appears only smaller icebergs can be detected using this method.

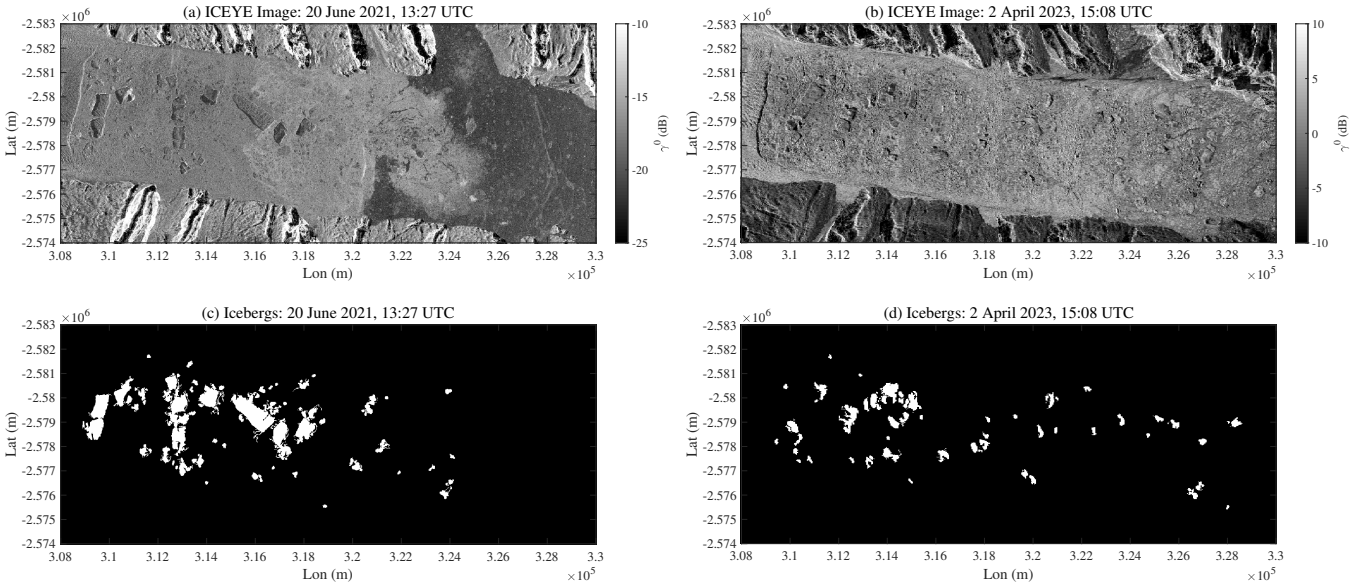

Fig. 6. Iceberg detection results using the texture-based method. The original ICEYE images in (a) summer and (b) winter are shown in the top panels, whilst the detection results are shown for (c) summer and (d) winter in the bottom panels.

ICEYE outperforms Sentinel-1 in segmenting icebergs using SAM, while both ICEYE and Sentinel-1 perform similarly at segmenting the mélange matrix. Sentinel-1 correctly classified 31% and 18% of icebergs compared to our manual digitization of icebergs (Figure 7). From ICEYE images taken within 24 hours of the Sentinel-1 images, ICEYE correctly classified 76% and 78% of icebergs. The time separation between the ICEYE and Sentinel-1 images was 4 (summer) and 19 (winter) hours, respectively. Assuming an iceberg displacment of $\sim$1 m per hour in summer, this leads to a movement of 4 m which is below the 10 m resolution of Sentinel-1 imagery and hence negligible to the accuracy statistics. We estimate an iceberg

displacement of ∼16 m in 19 hours during winter based on the accurate velocity data presented below, which is equivalent to 1.5 Sentinel-1 pixels. Therefore, validation of winter Sentinel-1 iceberg detections will be only marginally affected by this change. From Figure 8a, b, SAM can detect large ($\geqslant$ 1 km length) icebergs in the rigid matrix accurately, while many large icebergs were undetected in the Sentinel-1 imagery (Figure 8c, d). Within the non-rigid matrix farther away from the terminus, both ICEYE and Sentinel-1 imagery misclassified small areas of sea ice as an iceberg (identified visually), while a large area of sea ice in the downfjord area was misclassified in the ICEYE image from 8 March 2023 (Figure 8b). Both ICEYE and Sentinel-1 are able to detect smaller icebergs, particularly in the downfjord areas, and surprisingly the 20 March 2021 Sentinel-1 image detects more smaller icebergs compared to the ICEYE image of the same date (Figures 8a, c). Sentinel-1's low and inconsistent F1 scores of 0.42 and 0.27 (Figures 7c, d) likely stem from its coarser resolution compared to ICEYE. Unlike Sentinel-1, the ICEYE F1 scores of 0.76 and 0.78 (Figures 7a, b) indicate that SAM performed consistently well on ICEYE imagery.

Ice Mélange Velocity

The velocity comparison indicates that 6 out of 8 image pairs contain systematic offsets as demonstrated by the large mean values (μ) in Figure 9. For example, the velocity difference between 8 March 2023 to 12 March 2023 and the ATLAS data had a mean offset of $\mu = 20.8$ m (Figure 9b), indicating a systematic offset between the two SAR images. In comparison, the mean offset between 30 March 2023 to 2 April 2023 and ATLAS was 0.2 m, indicating that the misalignment between both images was minimal. The large value of μ for all but two velocity maps indicates the poor performance of ICEYE for tracking the movement of rigid ice mélange and is caused by a misalignment between the majority of the ICEYE images. In contrast, the uncertainty of each ICEYE mélange velocity map, indicated by the standard deviation (σ) of each distribution, is consistently below 5 m for 7/8 image pairs. This indicates that despite the systematic offset between the ICEYE images, the ImGRAFT feature tracking is able to compute the displacement between pixels with high accuracy. Visually, this is indicated by a narrow distribution for all histograms in Figure 9. Each histogram is normally distributed, indicating the presence of random errors in the feature tracking result, illustrating that the ICEYE SAR images can sufficiently track the movement of the matrix, but the results may only be reliable if the systematic offset can be corrected. We choose not to consider the velocity data further in this study for two reasons: (1) the systematic offset precludes analysis of velocity changes; and (2) the validation results only cover mélange near the glacier terminus, hence a correction

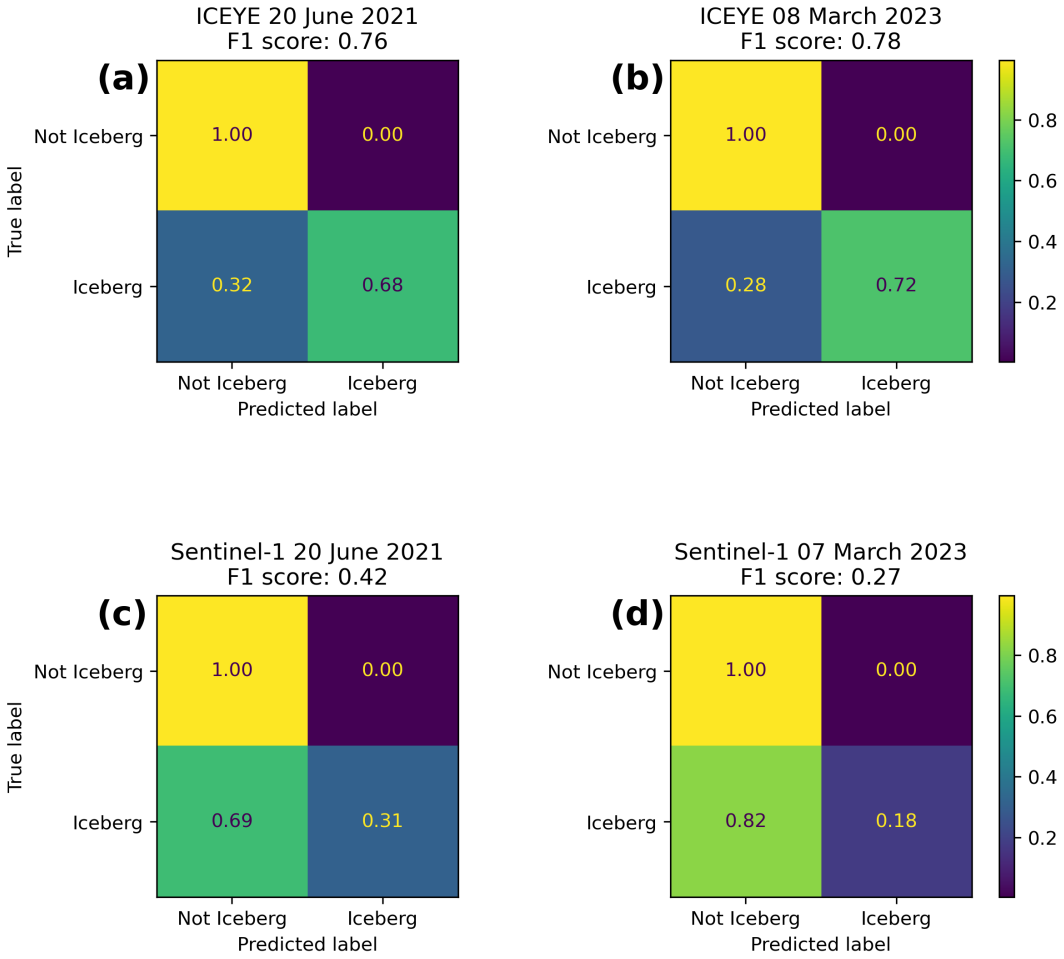

Fig. 7. Confusion matrices for ICEYE (a) summer and (b) winter and for Sentinel-1 iceberg segmentation using no prompt SAM in (c) summer and (d) 2023.

using μ would extrapolate results which may lead to errors.

DISCUSSION

Performance of Ice Mélange Monitoring with ICEYE

This study shows that ICEYE SAR imagery can be used to measure changes in the surface characteristics of ice mélange in both summer and winter through image texture. Radar backscatter from sea ice is generally larger at X-band compared to C-band (Johansson and others, 2018) and the smaller wavelength means it is more sensitive to changes in surface conditions. This means that as the surface melts or refreezes, icebergs flip over, and new sea ice forms, ICEYE will be able to detect these changes rapidly through textural variations across the image. These changes are most apparent in summer when the non-rigid

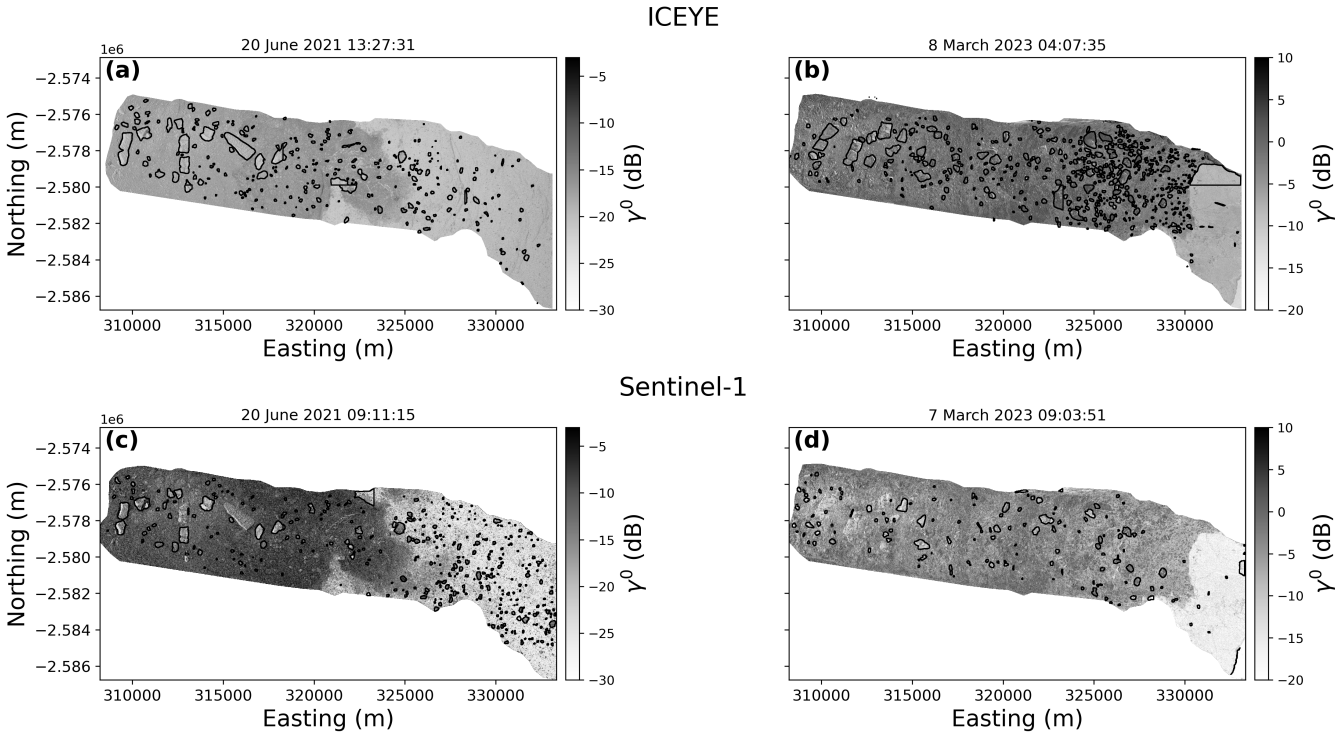

Fig. 8. Iceberg detection results using SAM. The results are overlaid on the ICEYE images in (a) summer and (b) winter. Similarly, the (c) summer and (d) winter Sentinel-1 results are shown in the bottom panel.

mélange melts and icebergs move around in response to fjord currents and wind patterns (Amundson and others, 2020). Air temperature at Mittivakkat glacier 80 km south of Helheim Fjord was above 0°C at the time of the summer ICEYE image acquisitions, suggesting the mélange surface may have been melting, evidenced by the negatively skewed summer distributions in Figure 4. In winter, the air temperature was -15°C, and the mélange surface was frozen; hence, radar backscatter was generally higher. This was further enhanced by the random assemblage of icebergs in the matrix evidenced by the Gaussian distribution in Figure 4, which increases the mélange roughness and hence radar backscatter. Whilst this analysis may be possible with optical imagery, it cannot be used in the Polar night or under cloudy conditions. In these conditions, ICEYE is preferred over Sentinel-1 due its higher spatial resolution, which enhances image textural variations and the shorter wavelength, whilst radar backscatter using ICEYE is more sensitive to surface changes.

We have also presented new techniques to segment large icebergs in the noisy mélange environment. Whilst the texture-based method is limited to working in summer when the mélange texture is more variable, SAM performs well in both seasons. For the texture-based method, further testing of post-segmentation filtering methods in fjords with different water depths and calving regimes is required in order

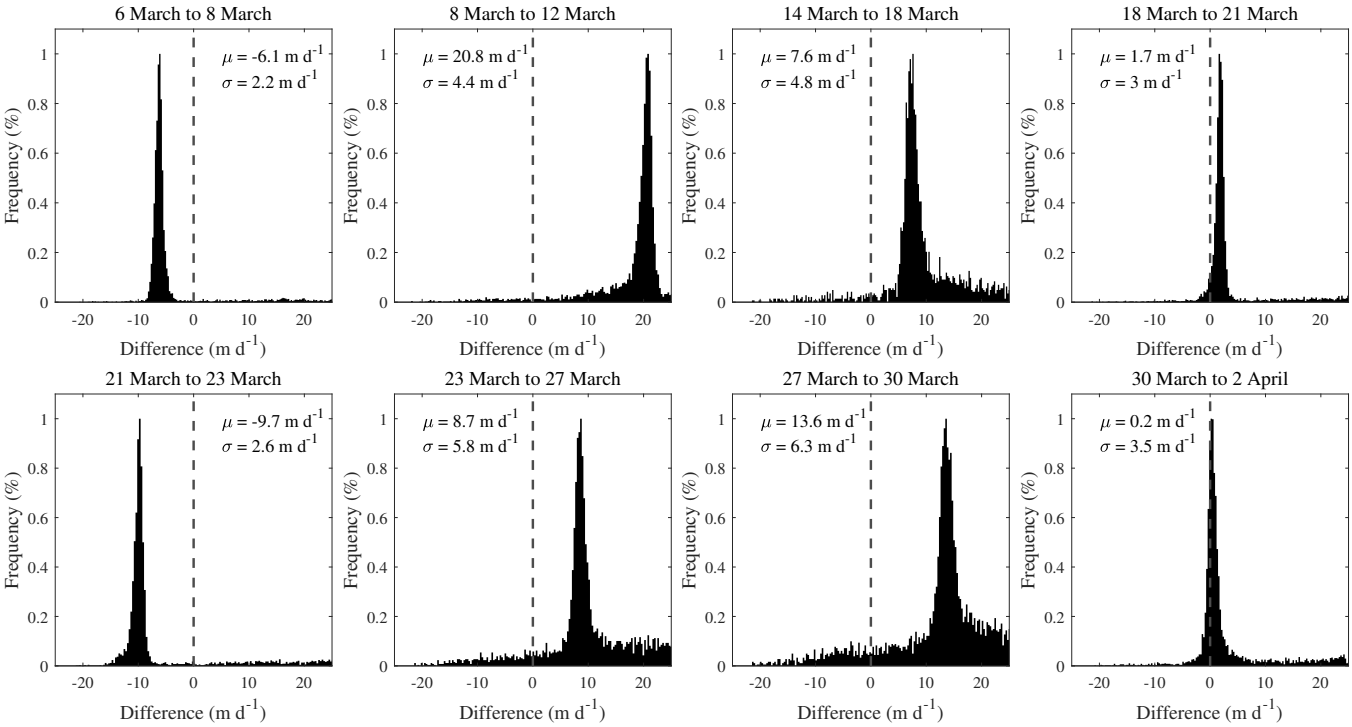

Fig. 9. Normalised histograms of the difference between ATLAS and ICEYE velocities for each of the ICEYE image pairs. Also stated for each histogram is the mean (μ) and standard deviation (σ). Black dotted line represents a mean of 0.

to automate the thresholding of thresholding of feature thicknesses (T) applied in this study. Furthermore, ICEYE outperforms Sentinel-1 for iceberg segmentation, which demonstrates that even with just a single polarisation, ICEYE requires less processing to achieve high classification accuracy. Previous studies have applied object-based image analysis methods, deep learning and semi-supervised clustering algorithms to SAR imagery to detect icebergs within sea ice (Mazur and others, 2017; Barbat and others, 2019; Færch and others, 2024). Shiggins and others (2023) applied a threshold to Digital Elevation Models (DEMs) to detect icebergs in the mélange, but 3D data are not widely available for routine iceberg mapping. Furthermore, dual-polarisation SAR sensors (e.g. Sentinel-1) can be used to mitigate the impact of sea surface waves, which may be misclassified as icebergs, hence ICEYE may not be suitable for open water iceberg detection as it only uses a single polarisation. Melting icebergs increase signal absorption and icebergs that have flipped have smooth undersides, which increases specular reflection, hence both processes reduces radar backscatter and lead to 'dark' icebergs with similar backscatter characteristics to open water. Both methods employed in this study were able to detect these icebergs in ICEYE imagery but not in Sentinel-1, demonstrating that high-resolution imagery leads to a significant improvement in detection accuracy, and with less pre-processing.

The geometry of the ICEYE image acquisition significantly impacts the performance of both the iceberg detection algorithms and velocity retrievals. For more accurate iceberg segmentation results using SAM, it is important to ensure the image patching matches the size of large icebergs, which may be >1 km in length. Ensuring this will reduce the amount of times an iceberg is split between different windows, limiting the artifacts produced from image patching. Furthermore, the systematic offset observed in the velocity results (Figure 9) is due to the poor geolocation accuracy after range-Doppler correction when using images from different orbits. Each image pair used to extract velocities contained images from different orbits, even in the case of velocities with small errors (Figures 9d and 9h). This suggests that the coregistration in SNAP did not sufficiently align the images to extract accurate velocities. The misalignment is due to the combination of DEM and geolocation errors in both images (Kääb and others, 2016), both of which will be large for the ICEYE imagery as more pixels require correction due to the high spatial resolution. This issue is less severe for Sentinel-1 as their orbits are well defined and repeat images can only be from one of two satellites in comparison to ICEYE. Therefore, improved methods to coregister ICEYE SAR images from different orbits and viewing geometries are required to improve the velocity mapping performance over both ice mélange and glaciers. This may also enable velocity mapping of ice mélange in summer, which is more difficult to achieve as the matrix is non-rigid and feature-tracking results tend to be non-coherent (Bevan and others, 2019).

Structural Evolution of Ice Mélange

The multi-zone structure revealed by the texture analysis (e.g., Figure 5) represents changes in radar backscatter that we suggest are due to changes in ice concentrations downfjord. In summer, the mélange matrix is non-rigid and icebergs move downfjord, melting along the way due to higher atmospheric and ocean temperatures, and leading to greater variations in image texture. For example, pixel values are lower nearer the terminus (zone 1) where we would expect higher concentrations of medium to large icebergs. In contrast, further down the fjord (zone 2), these icebergs break up into smaller fragments generating a rough surface profile that increases radar backscatter at X-band (Guo and others, 2023). The lower backscatter at the edge of the mélange (zone 3 in Figure 5a) relates to the increased presence of open water and sea ice, both of which are smoother and consequently increase specular reflection, whilst greater surface melt absorbs the ice signal. In comparison, structural zones in the winter mélange is less clear, with only two zones observed. We suggest this is due to the low air temperatures and lack of surface melting, which

ensures the mélange remains rigid and the iceberg texture remains consistent across multiple images.

The presence of structural zones with distinct ice concentration properties within the mélange implies that the boundary between them represents a lines of weakness within the granular matrix. Zones with high ice concentration will flow slower than zones with low concentration due to the combined effect of basal and atmospheric drag (Hughes, 2022). This leads to different flow rates which may lead to compressional or extensional flow. Turbulent water flow beneath the mélange (Hughes, 2022) could lead to flow in opposite directions between zones and the formation of a shear zone. Although our data cannot be used to quantify the flow regime of these different zones, their differences implies that the boundary between them represents a line of weakness in the mélange matrix. Applying this hypothesis to the winter imagery where we observe two zones and a line of weakness ∼10.1 km from the glacier terminus, we suggest that the ice mélange matrix contains structural weaknesses in both seasons that may persist throughout the year.

The presence of lines of weaknesses within ice mélange has not been documented before and could play an important role in determining the strength of the granular matrix. For example, Figure 10 shows a time series of a break-up event around the time of the 2021 summer images acquired from ICEYE. No structure can be observed in the optical imagery on 17 June, which is likely due to the lower contrast in ice concentration at visible wavelengths. From 17 to 20 of June 2021 the mélange begins to break apart. This coincides with the dates of the ICEYE imagery and confirms that the structural zoning is due to ice concentration differences. On 25 June, the mélange breaks up and the loose material moves down fjord. At this point, the higher concentration mélange remains pinned to the large iceberg, maintaining the line of weakness. Then, by 27 June, most of the low-concentration mélange has dispersed, leaving behind the high-concentration mélange near the terminus. This sequence serves to illustrate that the break-up of the matrix initiates at the open water boundary but terminates at the line of weakness created by the ice concentration differences. This shortens the mélange suddenly, potentially reducing the buttressing force on the tidewater glacier. Furthermore, the strong control of the high ice concentration zone on the mélange break-up suggests that length-width ratios (Burton and others, 2018; Schlemm and Levermann, 2021) might be misleading for the 'true length' included in backstress calculations and instead only the length of the high ice concentration area should be used. The observed control of structural zoning on ice mélange break-up strongly implies that this event, which may occur several times across the year, may be predictable if the lines of weakness can be detected. For example, they may cause and define the extent of winter mélange break up events (Cassotto and others, 2015). Therefore, high resolution SAR imagery

from ICEYE, which can detect these subtle ice concentration differences, has the necessary capabilities to monitor precursors to mélange break up, which has implications for understanding its strength and buttressing force on tidewater glacier termini.

The presence of large icebergs at the observed lines of weakness within the ice mélange suggests they are critical in determining the size of the structural zones and hence the strength of the matrix. In particular, our iceberg detection results indicate that they stabilise in the same location in both summer and winter. For example, two icebergs ∼1 km from the terminus appear in both summer and winter and likely originate from the calving of a large iceberg along the fracture lines that originate upstream of the terminus. The fact these icebergs remain in the same position over 7 days in summer and in Figure 10 for 10 days suggests they are pinned to a submarine sill. This appears to also be the case for the iceberg ∼10 km from the terminus, which is much larger. Although direct observations of the seafloor topography are scarce, the few direct observations from Helheim Fjord (An and others, 2019) suggest a bathyemetric sill could be present where the largest iceberg was detected ∼10 km from the glacier terminus. Furthermore, when icebergs remain stationary they fuse sea ice together (Robel, 2017; Cassotto and others, 2021) and ultimately bond the granular matrix. We therefore hypothesise that bathymetric sills represent the nucleus of structural zoning in the mélange by stabilising icebergs, restricting the outflow of ice and initiating sea ice growth. Whilst we have observed this process directly in summer, the Gaussian PDFs in winter suggest that icebergs are more randomly distributed and the structural zoning is suppressed, hence further work is required to understand the extent to which icebergs control the formation of structural weaknesses in the winter matrix.

Future Glaciological Opportunities for ICEYE & Small Satellites

There are only a handful of studies using ICEYE to monitor glaciers, with no published studies using the constellation to study icebergs or sea ice. Daily ICEYE acquisitions have been used to map grounding line changes at Petermann Glacier in northern Greenland and Thwaites Glacier in Antarctica using interferometry (Ciracì and others, 2023; Rignot and others, 2024). In both cases, the increased spatial and temporal resolution, as well as an improved interferometric baseline between successive satellite passes, increased the accuracy of the data products compared to satellites such as Sentinel-1. Meanwhile, Łukosz and others (2021) mapped the velocity of Sermeq Kujalleq (Jakobshavn Isbræ) using an ICEYE image pair with a temporal separation of 4 days in winter. They suggested that the results were of a comparable magnitude to Sentinel-1 velocities, but no comprehensive validation was conducted. The findings of these

Fig. 10. Ice mélange break up sequence spanning from 17 June through 27 June. Note the consistent rigid mélange shape closer to the terminus and the large tabular iceberg pinning the rigid mélange.

studies suggest that ICEYE has the potential to track surface displacements across ice mélange despite the poor performance of the feature-tracking reported in this study. Combined with the improved detection of

icebergs and the ability to monitor changes in surface characteristics, we find that ICEYE SAR imagery outperforms existing satellites such as Sentinel-1 and should be considered for future monitoring of glacier environments.

There are three key areas where the acquisition of daily ICEYE SAR images with a 2.5 spatial resolution can deliver significant new physical understanding: 1) iceberg calving, 2) supraglacial hydrological processes, and 3) glacial hazards. Firstly, ICEYE data may be employed to delineate tidewater glacier termini every day as well as the crevasse fields near the glacier terminus, both of which are crucial features in understanding calving rates and their drivers. Currently, coarse-resolution satellites (Zhang and others, 2023; Surawy-Stepney and others, 2023) or DEMs (Chudley and others, 2025) are used to map these features, neither of which can monitor the evolution of these features. Furthermore, the resulting icebergs may be tracked at higher temporal resolution, opening up the potential to infer near-surface ocean currents in glacial fjords. Secondly, because X-band radar backscatter from ice surfaces reduces as water content increases (Ulaby and others, 2019), it follows that the improvement in spatial and temporal resolution offered by ICEYE opens up the possibility to track melt patterns in greater detail than previously possible. This includes the onset and spatial evolution of melt over an annual cycle, as well as the complex distribution of supraglacial lakes and streams that form seasonally. Third and finally, several glacial hazards, such as glacial lake outburst floods (GLOFs) and ice avalanches, occur suddenly in time and can have fatal impacts, but only a handful are monitored by in situ instruments (Dematteis and others, 2021; Tiwari and others, 2022). ICEYE SAR imagery can be used to rapidly assess glacial hazards through tasking areas of interest and hence bridge the gap between ground and spaceborne monitoring. Whilst we believe there are numerous future applications of ICEYE, these three areas are particularly promising and should be an avenue for future development of ICEYE for cryosphere monitoring.

Despite the clear potential for using ICEYE for ice mélange and glacier monitoring, there are technical challenges that must be overcome. The orbits of each ICEYE satellite is different, therefore terrain distortions introduced by the side-looking SAR geometry varies between each satellite. Developing correction algorithms that effectively remove terrain distortions and accurately geocodes the resulting image, then fully validating these approaches, is crucial for exploiting the dense time series of observations that can be acquired through the ICEYE constellation. This is particularly important across ice mélange where a DEM matching the SAR image acquisition time is usually not available. Coregistering SAR images for feature-tracking is a related issue, and we found in this study that coregistration using SNAP performed

poorly, leading to large errors in the resulting velocity fields. Therefore, concurrently with the improvements in geometric image corrections, improved coregistration of ICEYE SAR images should be developed to enable more accurate velocity mapping. Furthermore, ICEYE uses a single polarisation, which reduces the diversity of information it can measure. This was observed when differentiating between large icebergs and the surrounding mélange in winter where the pixel values of the co-polarised backscatter did not vary significantly to enable the differentiation of each using the texture-based segmentation method. In this study, we use GLCM texture layers to enhance iceberg segmentation, but other texture-based methods such as Gabor transforms, wavelet transforms or edge detectors (Kandaswamy and others, 2005) or phase-based RGB composites (Arenas-Pingarrón and others, 2025) may help to improve the classification and segmentation of ice mélange image features. Finally, the texture-based iceberg segmentation method should be developed in the future as a tool to automatically label icebergs as training data (pseudo-labeling) for deep learning algorithms such as SAM to reduce the need for manual intervention in the training process.

There are several new and upcoming small satellite constellations with SAR (e.g. ICEYE, Capella, Umbra) and optical (e.g. Planet, Pléiades) payloads, as well as others developed by research groups (e.g. Dideriksen and others, 2024), that may be relevant for environmental monitoring. Several of these constellations acquire new imagery through tasking. For ICEYE, which now operates 50 satellites as of July 2025, it is possible to acquire several images a day in all seasons. However, high temporal resolution is only achieved by acquiring images from satellites in different orbits, causing variations in image texture that are due to satellite image viewing geometry rather than physical processes. This complicates image segmentation methods and other techniques such as interferometry. It should also be noted that there are usage limits on image tasking and satellites may be more frequently used to help with humanitarian aid and hazard warning during natural disasters and conflicts, thus reducing capacity for other users. Furthermore, ICEYE satellites can acquire images at 0.25 m (Spot), 2.5 m (Strip), and 15 m (Scan) resolution, but increasing spatial resolution reduces the spatial coverage of an image. Here, we used ICEYE Strip data which ensures coverage over the Helheim Glacier mélange at a high spatial resolution, but Spot data could have been acquired to focus on a smaller region of interest, such as mélange near the calving front. Therefore, the trade-off between spatial resolution and coverage depends on the downstream application. Finally, it remains unclear how well both the SAR and optical data from commercial and non-commercial small satellite payloads compare to widely used satellite data sets (e.g. Landsat, Copernicus satellites, ASTER, ALOS PALSAR) in different contexts. We have shown in this study that the poor geolocation

accuracy of ICEYE imagery inhibits mélange velocity mapping and this has also been shown for other small satellites such as Pléiades (Berthier and others, 2024) and Planet (Millan and others, 2019). Therefore, to fully exploit the potential of these new satellite constellations, we urgently need to conduct detailed validation studies and develop suitable algorithms to improve data quality.

CONCLUSIONS

In this study, we have used high-resolution ICEYE SAR imagery to map the dynamics of ice mélange in Greenland by mapping image texture, segmenting icebergs in the noisy mélange environment, and tracking the velocity of the matrix. Texture analysis reveals zoning within the mélange that relates to changes in ice concentrations downfjord. This structure is partially due to the stabilisation of large icebergs, potentially on submarine sills, which then act as the nucleus of sea ice formation whilst also preventing the downfjord flow of smaller icebergs. Lines of weakness are created within the matrix, and we show through a sequence of optical satellite images that the mélange breaks up at these locations through calving. The fact that this structure is present in both summer and winter suggests the mélange is susceptible to break-up throughout the year. Furthermore, we find that ICEYE outperforms Sentinel-1 when segmenting large icebergs in the mélange using the deep learning model SAM (Kirillov and others, 2023), suggesting that high-resolution SAR imagery improves iceberg monitoring. In contrast, poor coregistration betwen ICEYE images in different orbits leads to errors in velocity maps, rendering them unusable for tracking the dynamics of the mélange. Improved algorithms for image registration are required to develop ICEYE for monitoring ice mélange and glacier flow rates. Overall, the ability to acquire 2.5 m resolution SAR images at daily or subdaily resolution with large image swaths enables more detailed monitoring of highly dynamic processes and has the potential to be used in a range of glaciological applications e.g. hazard monitoring, understanding iceberg calving.

DATA AVAILABILITY

ATLAS data can be accessed via the Amazon Web Services (AWS) command line interface (https://aws.amazon.com/cli/) via the directory s3://atlas-lidar-helheim. All other data sets (2021 ICEYE images, labels, segmentation outputs) are available from the authors upon request.

ACKNOWLEDGEMENTS

We acknowledge funding to purchase ICEYE images in 2021 from the Scottish Alliance for Geoscience, Environment and Society (SAGES) International Collaboration Scheme (SICS) and access to ICEYE imagery in 2023 through the European Space Agency (ESA) Third Party Mission (TPM) scheme (Proposal ID: PP0089920). Leigh Stearns and Michael Shahin acknowledge funding from the Heising-Simons Foundation (HSF #2017-316) and NSF (BAA #00124801). ICEYE images from 2023 are available at https://tpm-ds.eo.esa.int/smcat/ICEYE/. WDH acknowledges the generous support of alumni and friends in establishing the University of Aberdeen's Interdisciplinary Institute. We would also like to thank Karen Alley (Scientific Editor) and one anonymous reviewer for their comments, which helped to improve the manuscript.

REFERENCES

Amundson JM and Burton J (2018) Quasi-static granular flow of ice mélange. *Journal of Geophysical Research: Earth Surface*, **123**(9), 2243–2257. (doi: 10.1029/2018JF004685)

Amundson JM and others (2020) Formation, flow and break-up of ephemeral ice mélange at LeConte Glacier and Bay, Alaska. *Journal of Glaciology*, **66**(258), 577–590. (doi: 10.1017/jog.2020.29)

Amundson JM, Fahnestock M, Truffer M, Brown J, Lüthi MP and Motyka RJ (2010) Ice mélange dynamics and implications for terminus stability, Jakobshavn Isbræ, Greenland. *Journal of Geophysical Research: Earth Surface*, **115**(F1) (doi: 10.1029/2009JF001405)

An L and others (2019) Bathymetry of southeast Greenland from oceans melting Greenland (OMG) data. *Geophysical Research Letters*, **46**(20), 11197–11205. (doi: 10.1029/2019GL083953)

Arenas-Pingarrón A and others (2025) An alternative representation of Synthetic Aperture Radar images as an aid to the interpretation of englacial observations. *EGUsphere*, **2025**, 1–21 (doi: 10.5194/egusphere-2025-1068)

Barbat MM, Wesche C, Werhli AV and Mata MM (2019) An adaptive machine learning approach to improve automatic iceberg detection from SAR images. *ISPRS Journal of Photogrammetry and Remote Sensing*, **156**, 247–259. (doi: 10.1016/j.isprsjprs.2019.08.015)

Berthier E and others (2024) The Pléiades Glacier Observatory: high-resolution digital elevation models and orthoimagery to monitor glacier change. *The Cryosphere*, **18**(12), 5551–5571. (doi: 10.5194/tc-18-5551-2024)

Bevan SL, Luckman AJ, Benn DI, Cowton T and Todd J (2019) Impact of warming shelf waters on ice mélange and terminus retreat at a large SE Greenland glacier. *The Cryosphere*, **13**(9), 2303–2315. (doi: 10.5194/tc-13-2303-2019)

Burton JC, Amundson JM, Cassotto R, Kuo CC and Dennin M (2018) Quantifying flow and stress in ice mélange, the world's largest granular material. *Proceedings of the National Academy of Sciences*, **115**(20), 5105–5110. (doi: 10.1073/pnas.1715136115)

Cassotto R, Fahnestock M, Amundson JM, Truffer M and Joughin I (2015) Seasonal and interannual variations in ice melange and its impact on terminus stability, Jakobshavn Isbræ, Greenland. *Journal of Glaciology*, **61**(225), 76–88. (doi: 10.3189/2015JoG13J235)

Cassotto RK, Burton JC, Amundson JM, Fahnestock MA and Truffer M (2021) Granular decoherence precedes ice mélange failure and glacier calving at Jakobshavn Isbræ. *Nature Geoscience*, **14**(6), 417–422. (doi: 10.1038/s41561-021-00754-9)

Chudley TR, Howat IM, King MD and MacKie EJ (2025) Increased crevassing across accelerating greenland ice sheet margins. *Nature Geoscience*, **18**(2), 148–153 (doi: 10.1038/s41561-024-01636-6)

Ciracì E and others (2023) Melt rates in the kilometer-size grounding zone of Petermann Glacier, Greenland, before and during a retreat. *Proceedings of the National Academy of Sciences*, **120**(20), e2220924120. (doi: 10.1073/pnas.222092412)

Cook S and others (2014) Modelling environmental influences on calving at Helheim Glacier in eastern Greenland. *The Cryosphere*, **8**(3), 827–841. (doi: 10.5194/tc-8-827-2014)

Davison B, Cowton T, Cottier FR and Sole A (2020) Iceberg melting substantially modifies oceanic heat flux towards a major Greenlandic tidewater glacier. *Nature communications*, **11**(1), 5983. (doi: 10.1038/s41467-020-19805-7)

Dematteis N, Giordan D, Troilo F, Wrzesniak A and Godone D (2021) Ten-year monitoring of the Grandes Jorasses glaciers kinematics. Limits, potentialities, and possible applications of different monitoring systems. *Remote Sensing*, **13**(15), 3005. (doi: 10.3390/rs13153005)

Dideriksen AK and others (2024) DISCO-2–an ambitious earth observing student CubeSat for arctic climate research. *Frontiers in Remote Sensing*, **5**, 1474560. (doi: 10.3389/frsen.2024.1474560)

Everett A, Murray T, Selmes N, Holland D and Reeve DE (2021) The impacts of a subglacial discharge plume on calving, submarine melting, and mélange mass loss at Helheim Glacier, south east Greenland. *Journal of Geophysical Research: Earth Surface*, **126**(3), e2020JF005910. (doi: 10.1029/2020JF005910)

584 Færch L, Dierking W, Hughes N and Doulgeris AP (2024) Mapping icebergs in sea ice: An analysis of seasonal SAR
585 backscatter at C-and L-band. *Remote Sensing of Environment*, **304**, 114074. (doi: 10.1016/j.rse.2024.114074)

586 Foga S, Stearns LA and Van der Veen C (2014) Application of satellite remote sensing techniques to quantify terminus
587 and ice mélange behavior at Helheim Glacier, East Greenland. *Marine Technology Society Journal*, **48**(5), 81–91.
588 (doi: 10.4031/MTSJ.48.5.3)

589 Fried M and others (2018) Reconciling drivers of seasonal terminus advance and retreat at 13 Central West Green-
590 land tidewater glaciers. *Journal of Geophysical Research: Earth Surface*, **123**(7), 1590–1607. (doi: 10.1029/
591 2018JF004628)

592 Guo W, Itkin P, Singha S, Doulgeris AP, Johansson M and Spreen G (2023) Sea ice classification of TerraSAR-X
593 ScanSAR images for the MOSAiC expedition incorporating per-class incidence angle dependency of image texture.
594 *The Cryosphere*, **17**(3), 1279–1297. (doi: 10.5194/tc-17-1279-2023)

595 Haralick RM, Shanmugam K and Dinstein IH (1973) Textural features for image classification. *IEEE Transactions*
596 *on systems, man, and cybernetics*, **6**, 610–621. (doi: 10.1109/TSMC.1973.4309314)

597 Howat IM, Box JE, Ahn Y, Herrington A and McFadden EM (2010) Seasonal variability in the dynamics
598 of marine-terminating outlet glaciers in Greenland. *Journal of Glaciology*, **56**(198), 601–613. (doi: 10.3189/
599 002214310793146232)

600 Huang L, Fischer G and Hajnsek I (2021) Antarctic snow-covered sea ice topography derivation from TanDEM-X
601 using polarimetric SAR interferometry. *The Cryosphere*, **15**(12), 5323–5344. (doi: 10.5194/tc-15-5323-2021)

602 Hughes KG (2022) Pathways, form drag, and turbulence in simulations of an ocean flowing through an ice mélange.
603 *Journal of Geophysical Research: Oceans*, **127**(6), e2021JC018228. (doi: 10.1029/2021JC018228)

604 ICEYE (2023) ICEYE Missions Brochure. Technical report, ICEYE

605 Johansson AM, Brekke C, Spreen G and King JA (2018) X-, C-, and L-band SAR signatures of newly formed sea
606 ice in Arctic leads during winter and spring. *Remote Sensing of Environment*, **204**, 162–180. (doi: 10.1016/j.rse.
607 2017.10.032)

608 Kääb A, Winsvold SH, Altena B, Nuth C, Nagler T and Wuite J (2016) Glacier remote sensing using Sentinel-2.
609 Part I: Radiometric and geometric performance, and application to ice velocity. *Remote sensing*, **8**(7), 598. (doi:
610 10.3390/rs8070598)

611 Kandaswamy U, Adjeroh DA and Lee MC (2005) Efficient texture analysis of SAR imagery. *IEEE Transactions on*
612 *Geoscience and Remote Sensing*, **43**(9), 2075–2083. (doi: 10.1109/TGRS.2005.852768)

Kirillov A, Mintun E, Ravi N, Mao H, Rolland C, Gustafson L, Xiao T, Whitehead S, Berg AC, Lo WY, Dollár P and Girshick R (2023) Segment anything. In *Proceedings of the IEEE/CVF International Conference on Computer Vision (ICCV)*, 4015–4026 (doi: 10.1109/ICCV51070.2023.00371)

Łukosz MA, Hejmanowski R and Witkowski WT (2021) Evaluation of ICEYE Microsatellites Sensor for Surface Motion Detection—Jakobshavn Glacier Case Study. *Energies*, **14**(12), 3424. (doi: 10.3390/en14123424)

Mankoff KD and others (2019) Greenland Ice Sheet solid ice discharge from 1986 through 2017. *Earth System Science Data*, **11**(2), 769–786. (doi: 10.5194/essd-11-769-2019)

Marochov M, Stokes CR and Carbonneau PE (2021) Image classification of marine-terminating outlet glaciers in Greenland using deep learning methods. *The Cryosphere*, **15**(11), 5041–5059. (doi: 10.5194/tc-15-5041-2021)

Mazur A, Wåhlin AK and Krężel A (2017) An object-based SAR image iceberg detection algorithm applied to the Amundsen Sea. *Remote Sensing of Environment*, **189**, 67–83. (doi: 10.1016/j.rse.2016.11.013)

Messerli A and Grinsted A (2015) Image georectification and feature tracking toolbox: ImGRAFT. *Geoscientific Instrumentation, Methods and Data Systems*, **4**(1), 23–34. (doi: 10.5194/gi-4-23-2015)

Miles VV, Miles MW and Johannessen OM (2016) Satellite archives reveal abrupt changes in behavior of Helheim Glacier, southeast Greenland. *Journal of Glaciology*, **62**(231), 137–146. (doi: 10.1017/jog.2016.24)

Millan R and others (2019) Mapping surface flow velocity of glaciers at regional scale using a multiple sensors approach. *Remote Sensing*, **11**(21), 2498. (doi: 10.3390/rs11212498)

Millan R, Dehecq A, Trouvé E, Gourmelen N and Berthier E (2015) Elevation changes and X-band ice and snow penetration inferred from TanDEM-X data of the Mont-Blanc area. In *2015 8th International Workshop on the Analysis of Multitemporal Remote Sensing Images (Multi-Temp)*, 1–4., IEEE (doi: 10.1109/Multi-Temp.2015.7245753)

Moon T, Joughin I and Smith B (2015) Seasonal to multiyear variability of glacier surface velocity, terminus position, and sea ice/ice mélange in northwest Greenland. *Journal of Geophysical Research: Earth Surface*, **120**(5), 818–833. (doi: 10.1002/2015JF003494)

Mouginot J and others (2019) Forty-six years of Greenland Ice Sheet mass balance from 1972 to 2018. *Proceedings of the national academy of sciences*, **116**(19), 9239–9244. (doi: 10.1073/pnas.1904242116)

Moyer A, Sutherland D, Nienow P and Sole A (2019) Seasonal variations in iceberg freshwater flux in Sermilik Fjord, southeast Greenland from Sentinel-2 imagery. *Geophysical Research Letters*, **46**(15), 8903–8912. (doi: 10.1029/2019GL082309)

642 Muff D and others (2022) The ICEYE constellation-some new achievements. In *2022 IEEE Radar Conference (Radar-*
643 *Conf22)*, 1–4., IEEE (doi: 10.1109/RadarConf2248738.2022.9764281)

644 Otosaka IN and others (2023) Mass balance of the Greenland and Antarctic ice sheets from 1992 to 2020. *Earth*
645 *System Science Data*, **15**(4), 1597–1616. (doi: 10.5194/essd-15-1597-2023)

646 Otsu N (1979) A threshold selection method from gray-level histograms. *IEEE transactions on systems, man, and*
647 *cybernetics*, **9**(1), 62–66. (doi: 10.1109/TSMC.1979.4310076)

648 Peters IR and others (2015) Dynamic jamming of iceberg-choked fjords. *Geophysical Research Letters*, **42**(4), 1122–
649 1129. (doi: 10.1002/2014GL062715)

650 Rignot E, Ciracì E, Scheuchl B, Tolpekin V, Wollersheim M and Dow C (2024) Widespread seawater intrusions
651 beneath the grounded ice of Thwaites Glacier, West Antarctica. *Proceedings of the National Academy of Sciences*,
652 **121**(22), e2404766121. (doi: 10.1073/pnas.2404766121)

653 Robel AA (2017) Thinning sea ice weakens buttressing force of iceberg mélange and promotes calving. *Nature*
654 *Communications*, **8**(1), 14596. (doi: 10.1038/ncomms14596)

655 Schlemm T and Levermann A (2021) A simple parametrization of mélange buttressing for calving glaciers. *The*
656 *Cryosphere*, **15**(2), 531–545. (doi: 10.5194/tc-15-531-2021)

657 Shankar S, Stearns LA and van der Veen CJ (2023) Semantic segmentation of glaciological features across multiple
658 remote sensing platforms with the Segment Anything Model (SAM). *Journal of Glaciology*, **70** (doi: 10.1017/jog.
659 2023.95)

660 Shepherd A and others (2020) Mass balance of the Greenland Ice Sheet from 1992 to 2018. *Nature*, **579**(7798),
661 233–239.., ISSN 1476-4687 (doi: 10.1038/s41586-019-1855-2)

662 Shiggins CJ, Lea JM and Brough S (2023) Automated ArcticDEM iceberg detection tool: insights into area and
663 volume distributions, and their potential application to satellite imagery and modelling of glacier–iceberg–ocean
664 systems. *The Cryosphere*, **17**(1), 15–32. (doi: 10.5194/tc-17-15-2023)

665 Simonsen SB, Barletta VR, Colgan WT and Sørensen LS (2021) Greenland Ice Sheet mass balance (1992–2020) from
666 calibrated radar altimetry. *Geophysical Research Letters*, **48**(3), e2020GL091216. (doi: 10.1029/2020GL091216)

667 Surawy-Stepney T, Hogg AE, Cornford SL and Hogg DC (2023) Mapping Antarctic crevasses and their evolu-
668 tion with deep learning applied to satellite radar imagery. *The Cryosphere*, **17**(10), 4421–4445. (doi: 10.5194/
669 tc-17-4421-2023)

Tiwari A and others (2022) Potential seismic precursors and surficial dynamics of a deadly Himalayan disaster: An early warning approach. *Scientific reports*, **12**(1), 3733. (doi: 10.1038/s41598-022-07491-y)

Ulaby F, Dobson MC and Álvarez-Pérez JL (2019) *Handbook of radar scattering statistics for terrain*. Artech House

Wehrlé A, Lüthi MP and Vieli A (2023) The control of short-term ice mélange weakening episodes on calving activity at major Greenland outlet glaciers. *The Cryosphere*, **17**(1), 309–326. (doi: 10.5194/tc-17-309-2023)

Xie S, Dixon TH, Holland DM, Voytenko D and Vaňková I (2019) Rapid iceberg calving following removal of tightly packed pro-glacial mélange. *Nature communications*, **10**(1), 3250. (doi: 10.1038/s41467-019-10908-4)

Zhang E, Catania G and Trugman DT (2023) AutoTerm: an automated pipeline for glacier terminus extraction using machine learning and a "big data" repository of Greenland glacier termini. *The Cryosphere*, **17**(8), 3485–3503. (doi: 10.5194/tc-17-3485-2023)